Micromechanical basis for shear strength of rock discontinuities

A. Serrano, C. Olalla, R.A. Galindo

A B S T R A C T

The theoretical basis for evaluating shear strength in rock joints is presented and used to derive an equation that governs the relationship between tangential and normal stress on the joint during situations of slippage between the joint faces. The dependent variables include geometric dilatancy, the instantaneous friction angle, and a parameter that considers joint surface roughness. The effect roughness is studied, and the aforementioned formula is used to analyse joints under different conditions. A mathematical expression is deduced that explains Barton's value for the joint roughness coefficient (*JRC*) according to the roughness geometry. In particular, when the Hoek and Brown failure criterion is used for a rock in the contact with the surface roughness plane, it is possible to determine the shear strength of the joint as a function of the relationship between the uniaxial compressive strength of the wall with the normal stress acting on the wall. Finally, theoretical results obtained for the geometry of a three-dimensional joint are compared with those of the Barton's formulation.

Keywords:
Rock joint
Roughness
Shear strength
Theoretical model
Dilatancy

1. Introduction

Determining the shear strength of rock joints requires understanding the relationship between the mean normal stress on the rupture plane (mid-plane of the discontinuity) and the mean tangential stress produced by the slippage between the two rock faces. The study of the mechanical behaviour of joints has long attracted interest because it governs physical instability phenomena (slopes, tunnels, etc.) when configured by discontinuities. There are many studies that present constitutive theoretical and empirical models with which to simulate joint behaviour.

The aim of this article is to present several theoretical formulations that allow for the definition of shear strength in rock joints. This aim was accomplished by developing a theoretical model capable of capturing the primary mathematical structure of the equation that was reported in 1973 by Barton [1] and the dependence of the variables used in the description of this equation.

2. Background

One of the first models was proposed by Patton [2] in 1966 and was based on tests that were performed on artificially created joints in gypsum material, which were based on a saw-tooth pattern. The study verified results that were adjusted by Newland and Alley [3] according to a bilinear law that attempted to describe the dilatancy of granular materials. Similar models, in which a transition curve was adjusted between lines that corresponded to dilatancy and shear mechanisms, were proposed by Ladanyi, Archambault [4] and Jaeger [5] and were based on empirical models.

Shortly thereafter, more complex models began to appear. Some models compared the angles that defined surface roughness by normal stress [6], while others tried to predict the dilatancy phenomenon using the fracturing of joints subjected to tangential loads. However, it was Barton [1] who had the most success by incorporating into his dilatancy prediction study an empirical formula that considered the effects of joint roughness and dependence on the load level. Heuze and Babour [7] introduced a three-parameter model to predict the dilatancy produced in rock joints by empirically identifying a critical point, beyond which there was no dilatancy. Additionally, Leichnitz [8] developed a model that was capable of considering rock fractures produced by nonlinear behaviour in the material based on experimental results from sandstone.

From the saw-tooth roughness model first used by Patton, Plesha [9] formulated a constitutive model based on classical plasticity theory that incorporated an exponential degradation factor for roughness. Zubelewicz et al. [10] also studied degradation, and some years later, Qiu et al. [11] revised Plesha's model by considering sinusoidal instead of saw-tooth roughness. Saeb and Amadei [12] conducted a similar study based on an empirical ratio of the dilatancy factor that was given in 1970 by Ladanyi and Archambault [4], and in this manner, they described normal joint

displacement based on tangential displacement and normal stress. Seidel and Haberfield [13] evaluated plastic deformations produced by surface roughness shear by estimating joint dilatancy according to the energetic considerations produced by internal friction. Other investigations of the degradation of roughness in contacts between joint faces were performed by Hutson [14], Hutson and Dowding [15], Huang et al. [16], Lee et al. [17] and Homand et al. [18], among others.

Gens et al. [19] proposed an elastoplastic constitutive model to describe the three-dimensional behaviours of fractures. Similarly, Desai and Fishman [20] used plasticity theory to create constitutive equations that characterised the mechanical responses of fractures under loading, unloading, and reloading conditions.

More recently, Grasselli [21] and Belem [22] have formulated models to account for parameters that consider the three-dimensional natures of joint surfaces. A generalised three-dimensional formulation was created by Samadhhiya et al. [23] to account for joint dilatancy, roughness, and the undulation of discontinuous surfaces.

Among the existing models, Barton's empirical method [1,24,25] is likely the most widely used in practice. This method is based on the selection of the joint roughness coefficient (*JRC*) value, for which various approaches have been proposed to relate this value to the morphologies of the profiles that it defines; these approaches have also evaluated the use of fractal analysis [26–30], or statistical analysis [31], among other procedures.

Asadollahi [32] introduced a modification of the original Barton's shear failure criterion, which was based on limitations in Barton's criterion concerning the estimation of peak displacement or post-peak shear strength.

3. Failure mechanisms

The interaction between two surfaces in contact initially occurs at a finite number of points through a small number of atoms in their respective crystalline structures. These contact points are constituted by the peaks of the rough surfaces.

Terzaghi [33] proposed that the normal load acting on two bodies in contact causes the plastification of the corresponding surface roughnesses, wherein real contact takes place between the two bodies such that the frictional force is proportional to the normal force and is independent of the size of the two bodies in contact. The explanation of these empirical findings constitutes the Terzaghi adhesion theory. However, not all contacts must be plastified. Some contacts might experience elastic forces such that when the load increases, the elastic elements will slowly become plastic, while new elastic state contacts might appear simultaneously. The contact behaviour in the elastic state can be estimated by Hertz's law [34] of two elastic spheres in contact.

When accounting only for irregularities of this order, it is not possible to correctly model the shear strength of joints, as the shear strength force depends on both the strength of the particles that constitute the rock and the strength of the rock matrix at a higher hierarchical level. The manner in which these mechanical characteristics are connected to joint strength depends on the morphology and, in particular, the roughness of the joint. Thus, various successive degrees of roughness can present themselves on the surface of a rock and could be modelled with a fractal surface if they are statistically self-similar.

It is therefore necessary to consider a higher geometrical model than that described above; this model can be created supposing a simple geometry for the joint profile. In this sense, saw-tooth profiles have been commonly used in theoretical and experimental studies. Obviously, the joint profile can be modelled using more realistic models than the saw-tooth. In any case, for joint movement, the need to retain the geometric roughness implies a greater degree of energy consumption than would be necessary if there were only irregularities of a lower hierarchical rank, such as those described herein.

When contact occurs through surface roughness, two failure mechanisms result. In the first mechanism, the joint slips and forms angle α with the mid-plane of the joint (Fig. 1); this mechanism is used for low normal loads. In the second mechanism, the roughness is plastified and breaks (Fig. 1); this is used for high normal exterior loads.

The critical normal load N_{crit} discriminates between both mechanisms such that for normal stresses below this critical load, failure occurs through the first mechanism; the second mechanism applies to loads above the critical level (Fig. 2).

3.1. First mechanism analysis

It is considered the *i*th contact between the roughnesses according to the joint profile. It is assumed that the tangential plane in the *i*th contact forms the maximum angle α_i with the mid-plane of the joint in a section over the vertical plane, Π_i, that is perpendicular to the mid-plane in the direction of the shear load. Slippage is produced when

$$\frac{T_i^*}{N_i^*} \geq \tan \varphi_b \tag{1}$$

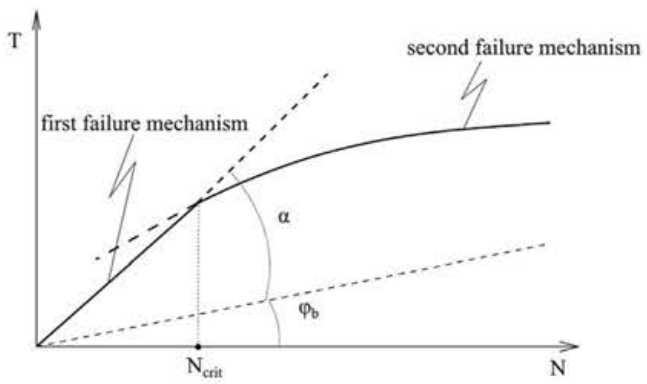

Fig. 2. Peak shear strength governing law.

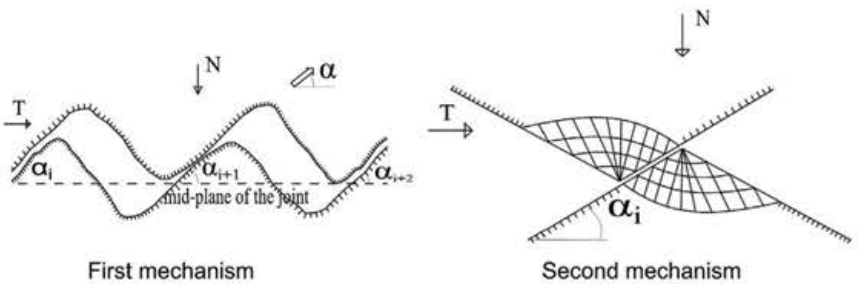

Fig. 1. First failure mechanism (slippage) and second failure mechanism (plastification of the contacts).

where φ_b is the basic friction angle of the material and T_i^* and N_i^* are the tangential and normal force in the contact on the tangential plane between the two surfaces, respectively, which are contained in plane Π_i (Fig. 3a).

If the forces contained in the plane Π_i for contact in the direction of the mid-plane and its normal are T_i and N_i respectively, then the relationship between the forces in both axis systems is

$$T_i^* = T_i \cos \alpha_i - N_i \sin \alpha_i \tag{2}$$

$$N_i^* = T_i \sin \alpha_i + N_i \cos \alpha_i \tag{3}$$

In a critical slippage situation, the equation terms will be equal (1); however, when substituting (2) and (3) and grouping terms, the following relationship between the tangential and normal forces in the global axes system is obtained:

$$\frac{T_i}{N_i} = \frac{\cos \alpha_i \tan \varphi_b + \sin \alpha_i}{\cos \alpha_i - \sin \alpha_i \tan \varphi_b} = \tan(\varphi_b + \alpha_i) = \tan(\varphi_p)_i$$

If these arguments are extended to the n contacts between the joint faces and a uniform distribution of force per unit of surface is assumed, it is possible to obtain the joint shear strength governing law according to the first mechanism described above:

$$\frac{\tau}{\sigma_n} = \tan(\varphi_B + \alpha) \tag{4}$$

with the value of angle α obtained via:

$$\alpha = -\varphi_b + \operatorname{atan}\left(\frac{\sum_1^n \tan(\varphi_b + \alpha_i)}{n}\right) \tag{5}$$

Alternatively, based on a statistical distribution of the slope angles formed by tangents to the roughness according to the Π_i plane, it is expressed:

$$\alpha = -\varphi_b + \operatorname{atan}\left(\frac{\tilde{\tau}}{\sigma_n}\right) \tag{6}$$

with

$$\left(\frac{\tilde{\tau}}{\sigma_n}\right) = \int_{\alpha_0}^{\alpha_f} \tan(\varphi_b + \alpha_i) f(\alpha_i) d\alpha_i$$

Such that $f(\alpha_i)$ is the density function for the angle α_i, and α_0 and α_f are the possible lower and upper limits of the slope angles.

The practical way to approach this first slippage mechanism includes the assumption of a constant average slope for each contact, although the contacts might differ from one another according to the measures that one can obtain or the estimated distributions of the angles of the slopes. Thusly, it is supposed that slippage is produced along a plane formed by angle α and the mid-plane according to Eqs. (5) and (6). Thus, movement between the joint walls is produced with constant dilatancy according to this angle; this phenomenon is defined as geometric dilatancy because it is produced by the geometry of the joint surface.

When using average slopes, there will be a distribution of the α_i angles for the roughness. Lacking more precise data, it is possible adjust these angles with a density function of beta distribution. Among all possible slopes, there will be some for which $\alpha_i \geq \alpha_l$ with $\alpha_l = \pi/2 - \varphi_b$. Substituting the value α_l of the slope in Eq. (4) is observed that the strength is infinite relative to the first failure mechanism. To break the joint with a shear force, it is necessary the bias of the roughnesses $\alpha_i \geq \alpha_l$. The final effect of these roughnesses is shear stress without normal force: in other words, a cohesive force.

In a practical analysis of the first mechanism, slippage occurs along the planes of the α_i angle, which is predefined in each one of the contacts. A specific distribution of these planes implies a certain expected strength law for the joint. Thus, when calculating the normal load, the contacts are plastified such that the contact surfaces are created with their respective roughnesses. It is possible to interpret this equilibrium as occurring in an ideal scenario for a joint with a saw-tooth profile, with variable slopes for each tooth according to a particular distribution.

Analysing this mechanism in terms of more realistic surfaces on which the closer the peaks of each irregularity are to each other, the more flattened the slope becomes. In this case, the above-described equations are verified in each equilibrium state by varying the angle of the slope at the contact along the joint opening u_n (Fig. 3b). This supposes the variation of the strength law of the first mechanism with the relative displacement produced between the joint faces. This geometrical configuration, produced mainly from damage to the asperities, allows to explain strength reduction such that when failure via slippage occurs with a constant normal load, the strength against tangential stress is lower due to that the contact angle will be smaller in a higher position. Thus, for joints in which this first mechanism of failure via slippage is produced, the space that constitutes the height of the contacts changes from peak strength to basic or residual distance. At this point, the geometric dilatancy is null (Fig. 4). However, from a practical perspective, it is possible consider the slope α_i for each roughness at a constant value and also the value of the average contact angle θ_i.

3.2. Analysis of the second mechanism

The interaction between the edges of a joint is composed of a large number of contact points such that the force is transmitted through these points. Failure can occur when the load on each contact is sufficiently high (Fig. 1). This situation can be

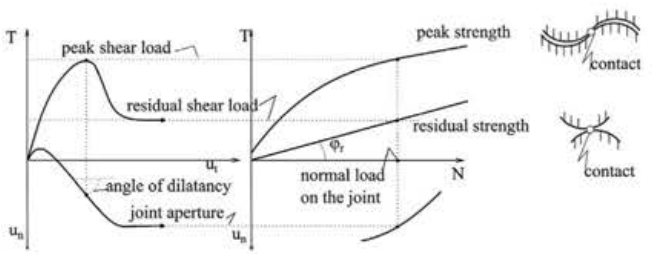

Fig. 4. Influence of surface roughness smoothing along the opening of the joint.

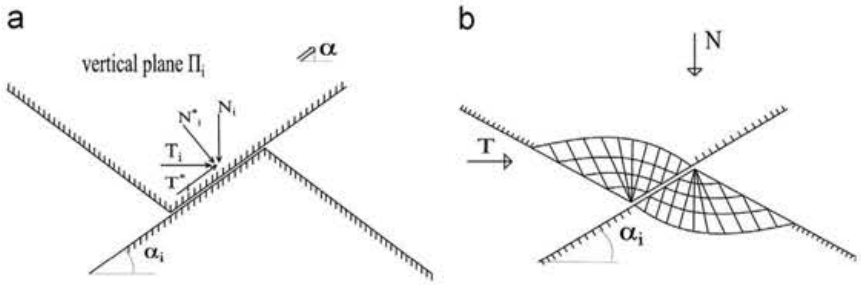

Fig. 3. (a) Contact forces according to the first failure mechanism; (b) Equilibrium situation for the first mechanism along the opening.

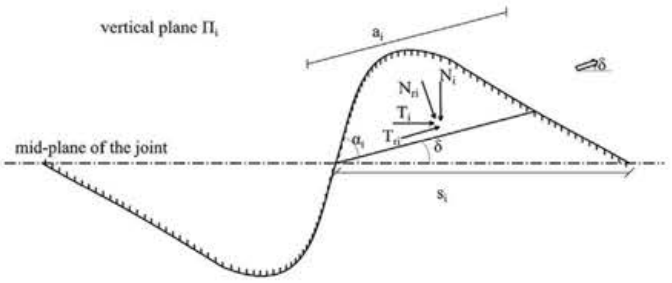

Fig. 5. Equilibrium of forces in the second failure mechanism.

mathematically modelled by supposing that the geometry of the joint can be defined by a particular surface roughness profile and adopting some hypotheses indicated below.

It is considered that the rock matrix obeys the shear strength governing law: $\tau = \tau(\sigma)$. It is assumed that when failure is produced by this mechanism, the joint moves with a dilatancy that is defined by the angle δ. The fracture surface for each given roughness is flat. The failure planes form a maximum angle with the mid-plane of the joint over vertical plane Π_i (perpendicular to the mid-plane in the direction of shear load). This angle, called dilatancy, is equal to δ (Fig. 5). Another hypothesis is that the fracture area α_i of each contact depends on the dilatancy angle δ, according to a particular angle $\alpha_i(\delta)$. One last hypothesis is used: rupture is produced for a dilatancy angle δ that minimises the total shearing force T of the failure for a certain constant normal load N over the joint. This condition can be mathematically expressed as

$$\left(\frac{\partial T}{\partial \delta}\right)_{N=\text{const}} = 0 \tag{7}$$

with $T = \Sigma T_i$.

Based on these hypotheses, the joint shear strength governing law can be mathematically deduced to relate the joint-plane stresses τ and the normal stress σ_n for the second failure mechanism as follows.

Failure equilibrium is produced for each contact according to the plane forming angle δ (failure plane) with the mid-plane of the joint over plane Π_i and indicates geometric dilatancy at failure. Fig. 5 expresses equilibrium in the contact according to the following expressions:

$$T_{ri} = T_i \cos\delta - N_i \sin\delta$$

$$N_{ri} = T_i \sin\delta + N_i \cos\delta$$

in which T_{ri} and N_{ri} are the failure loads on plane Π_i of the contact in the directions marked by the failure plane and its normal state, respectively, and T_i and N_i are the failure loads on the contact in the directions of the external loads acting on the joint.

For this mechanism, tangential (τ_{ri}) and normal (σ_{ri}) stress for each contact on the failure plane can be obtained with the following expressions:

$$\tau_{ri} = \frac{T_i \cos\delta - N_i \sin\delta}{a_i} \tag{8}$$

$$\sigma_{ri} = \frac{T_i \sin\delta + N_i \cos\delta}{a_i} = \frac{T_i \sin\delta}{a_i} - \frac{\tau_{ri}\cos\delta}{\sin\delta} + \frac{T_i \cos^2\delta}{a_i \sin\delta} \tag{9}$$

The derivatives of the stress in the dilatancy plane can be obtained based on Eqs. (8) and (9), resulting in:

$$\frac{d\tau_{ri}}{d\delta} = \frac{d\tau_{ri}}{d\sigma_{ri}}\frac{d\sigma_{ri}}{d\delta} = \tan\rho\frac{d\sigma_{ri}}{d\delta} \tag{10}$$

in which ρ is the instantaneous friction angle.

$$\frac{d\sigma_{ri}}{d\delta} = \frac{T_i - N_i \tan\kappa}{a_i \cos\delta \tan\kappa(\tan\delta + \tan\rho)} \tag{11}$$

Angle κ is defined as the reduction of the average contact area, such that:

$$\frac{1}{\tan\kappa} = \frac{-1}{a_i}\frac{da_i}{d\delta} \tag{12}$$

The tangential load T_i can be easily expressed by the equation:

$$T_i = \frac{\tau_{ri}a_i + N_i \sin\delta}{\cos\delta}$$

To apply the failure condition formulated in (7), it is necessary to calculate the expression of the derivative of each T_i for a particular value of constant normal load:

$$\left(\frac{\partial T_i}{\partial \delta}\right)_{N=\text{const}} = N_i + T_i \tan\delta - \frac{a_i}{\cos\delta}\left(\frac{\tau_{ri}}{\tan\kappa} - \frac{d\tau_{ri}}{d\delta}\right) \tag{13}$$

By substituting the expressions (8), (10) and (11) into (13), it is obtained:

$$\begin{aligned}\left(\frac{\partial T_i}{\partial \delta}\right)_{N=\text{const}} &= N_i\left(\frac{\tan^2\delta(1 - \tan\kappa\tan\rho) + \tan\delta(\tan\kappa + \tan\rho)}{\tan\kappa(\tan\rho + \tan\delta)}\right) \\ &\quad + T_i\left(\frac{\tan^2\delta(\tan\kappa + \tan\rho) - \tan\delta(1 - \tan\kappa\tan\rho)}{\tan\kappa(\tan\rho + \tan\delta)}\right)\end{aligned}$$

By extending this reasoning to n joint contacts such that the load per unit of surface is considered constant, with s_i representing the shear area for the mid-plane of the joint and $s_t = \Sigma_1^n s_i$, the following is obtained:

$$\begin{aligned}\left(\frac{\partial T}{\partial \delta}\right)_{N=cte} &= N\left(\tan\delta\left(\frac{1}{s}\Sigma_1^n\frac{s_i}{\tan\kappa_i}\right) + \frac{\tan\delta(1 - \tan\delta\tan\rho)}{(\tan\rho + \tan\delta)}\right) \\ &\quad + T\left(\tan\delta + \frac{-\tan\delta(1 - \tan\delta\tan\rho)}{(\tan\rho + \tan\delta)}\left(\frac{1}{s}\Sigma_1^n\frac{s_i}{\tan\kappa_i}\right)\right)\end{aligned} \tag{14}$$

By using the failure condition (7) and setting (14) equal to zero, the following is obtained:

$$\begin{aligned}\frac{\tau}{\sigma_n} = \frac{T}{N} &= \frac{((\tan\rho + \tan\delta)/(\tan\kappa_m)) + (1 - \tan\delta\tan\rho)}{((1 - \tan\delta\tan\rho)/(\tan\kappa_m)) - (\tan\rho + \tan\delta)} \\ &= \frac{\tan(\delta+\rho) + \tan\kappa_m}{1 - \tan(\delta+\rho)\tan\kappa_m} = \tan(\rho + \kappa_m + \delta)\end{aligned} \tag{15}$$

in which δ is the dilatancy angle at failure, ρ is the instantaneous friction angle and κ_m is the angle that represents the reduction in the area of contact in the joint, such that:

$$\frac{1}{\tan\kappa_m} = \frac{1}{s_t}\Sigma_1^n\frac{s_i}{\tan\kappa_i} \tag{16}$$

The value of κ_i should be obtained from the geometric properties of the different roughness values, according to what is indicated in Section 5. Thus, α^j with $j = 1,\ldots,m$ are independent geometric variables that define each irregularity, and each has an independent statistical distribution. Thus, it is expressed $\kappa_i = \kappa_i(\alpha^1,\ldots,\alpha^m)$, and if these values meet the mathematical conditions of derivability in each of the geometric variables that physically define roughness, then the value of the angle κ_m can be obtained as follows:

$$\frac{1}{\tan\kappa_m} = \int_{s_o}^{s_f}\int_{\alpha_0^m}^{\alpha_f^m}\cdots\int_{\alpha_0^1}^{\alpha_f^1}\frac{f(s_i)f(\alpha_i^1)\ldots f(\alpha_i^m)}{\tan(\kappa_i(\alpha_i^1,\ldots,\alpha_i^m))}ds_i d\alpha_i^1\ldots d\alpha_i^m \tag{17}$$

in which $f(\alpha_i^j)$ and $f(s_i)$ are the density functions of the geometric variable α^j and area s_i of contacts, respectively, and α_0^j and α_f^j are

the possible lower and upper limits, respectively, of these geometric variables, depending on the function κ_i. The lower and upper limits of the variable s_i are s_o and s_f, respectively.

4. Barton's empirical method (1973)

In 1973, Barton [1] formulated the law governing the shear strength of a rock joint from the following empirical equation:

$$\frac{\tau}{\sigma_n} = \tan(\varphi_b + \delta + f) = \tan \varphi_p \tag{18}$$

in which τ and σ_n are the stresses at the onset of failure according to the tangential and normal angles, respectively, and φb is the basic friction angle of the "healthy" joint wall, δ is the dilatancy angle achieved at the onset of joint movement, and f is a parameter that depends on roughness.

Barton [1] experimentally studied the relationship and found:

$$\varphi_p - \varphi_b = JRC \log \frac{JCS}{\sigma_n} \tag{19}$$

in which the joint roughness coefficient (*JRC*) is a coefficient that depends on surface roughness, and *JCS* represents the joint wall compressive strength of the rock wall.

When the joint surfaces are altered, the roughness is smoothed, and dilatancy disappears. In this case, the residual friction angle φ_r is reached, and $\varphi_b = \varphi_r$ (in principle; throughout this text, this will be considered as the basic friction angle. However, this angle coincides with the residual value when there are conditions of joint surface alteration). However, a scale effect can be considered for the tests of the *JRC* and *JCS* values when using correcting equations [35].

It must be noted that, according to Eq. (19), very high peak friction angles are found for very low compressions on the joint. As a result, the use of this relationship in Barton's formalism [1] tends to be restricted to σ_c/σ_n values greater than 50 to 100 and for those that have a constant and independent friction angle from the load valued:

$$\varphi_p = \varphi_b + 1.7JRC \tag{20}$$

Formula (15) can predict the value of the shear strength of the rock joint at failure in a manner similar to that obtained experimentally by Barton [1], as the variables on which this function depends also reference similar factors.

Eq. (18) depends on the basic friction angle of the joint wall (φ_b), the dilatancy angle (δ) and the roughness characteristics (f), while in the theoretical formula shown above, Eq. (15), the shear strength of the joint is a function of the instantaneous angle of roughness (ρ), the geometric dilatancy (δ) and the degree of reduction in the contact area and is dependent on geometric properties that define roughness (κ_m). The observed similarity is not random but rather the result of an adequate consideration of the factors that contribute to joint failure through the presented hypothesis and theoretical formulation.

The following sections will show how to consider the influence of roughness in the formula; in addition, as it was formulated by Barton's equation, dilatancy is set as a function of the relationship between the normal stress that acts on the joint and the uniaxial compressive strength.

5. Influence of roughness geometric factors

The influences of surface roughness shape and geometry on the second failure mechanism are clearly shown in this theoretical formulation using the component of reduction of contact area. In the case of Barton's empirical formula, the influence of surface roughness on the strength law was articulated with the *JRC* index, which in its initial formation was determined according to the similarity of the real joint to standard roughness profiles. Subsequently, to improve the objectivity of the estimate, statistical and fractal methods were suggested that supported correlations of this index with the parameters of the joint roughness profile [26–31].

Each of the geometric variables that were chosen to define each irregularity has a range of variation throughout the joint for different values of the contact roughness produced between the two faces of the discontinuity. This variation can be quantified by a particular distribution function, as indicated above.

In 1966, Dickey [36] used the profilometer technique and found that the polished surfaces of quartz crystals had average roughness heights of 0.5 μm and angles of 177° relative to the mid-plane. For rough quartz, the average height could be estimated in values of 5 μm at angles of approximately 120° (that is, values of the angles tangential to the irregularity over the mid-plane of 30°). The smoothest natural surfaces possible are those obtained through exfoliation and cleavage; even in the case of mica, the surface is undulated with roughness heights of up to 1 μm. Thus, a simple and representative formula to represent the roughness of a rock surface can be constructed from the measures of height h_i and amplitude b_i for each roughness such that the average contact angle of the irregularity θ_i may be represented as $\tan \theta_i = 2h_i/b_i$.

A geometric representation of roughness in the form of a harmonic profile might be useful. In this case, this profile can be defined from the slope of contact and the amplitudes over the mid-plane. Additionally, this could be used to define other more general profiles based on harmonic development in series.

A simplified study consists of the supposition of simple shapes for irregularities, including saw-teeth or softened curves that form circumference arcs, such that the roughness can be determined from a single parameter. Thus, for the simplest cases, such as the saw-tooth, it sufficient to use the slope angle for each roughness. In this sense, it is necessary to note that the selection of an adequate geometric parameter would permit the simultaneous characterisation of the first and second failure mechanisms. However, the analysis of the first mechanism would include the slope of the contact plane between the roughnesses.

When using a geometry in a plane perpendicular to the mid-plane of the joint and in the direction of shear load to model the roughness of the joint (as a plane deformation problem), this will be indicated that is used a profile linear roughness, as in the case of saw-tooth profiles.

Next, the dependence κ_i of the angle of reduction for each contact can be deduced for the various geometries used to define the joint profiles, as follows:

5.1. Geometry of linear surface roughness in saw-tooth form

The use of a saw-tooth joint profile assumes work in a plane deformation problem. Consequently, in a plane perpendicular to the joint plane that contains the shear load direction, the failure plane as forming a dilatancy angle δ with the mid-plane and the angles of the flat walls of the roughness with the mid-plane can be represented. These angles do not necessarily have to be symmetrical in the two roughness faces and thus can be considered more generally, such that when the contact face coincides with the tangential plane for contact i, angles α_{1i} and α_{2i} are formed, as shown in Fig. 6a. Assuming a unit length perpendicular to the plane represented in the figure, the sine theorem is applied to the *ABC* triangle, and thus, the following equation is obtained:

$$\frac{a_i}{\sin \alpha_{2i}} = \frac{s_i}{\sin(\pi - \alpha_{2i} - \delta)} \tag{21}$$

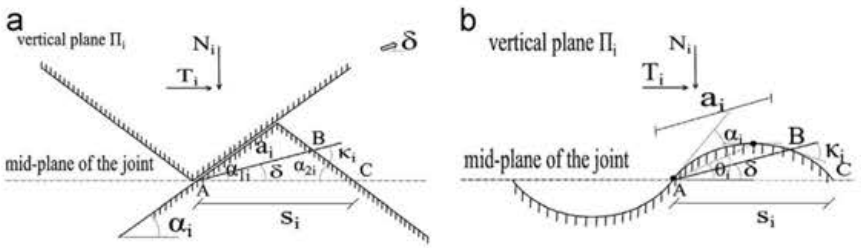

Fig. 6. (a) Saw-tooth rupture in contact *i*; (b) Linear surface roughness according to the circumference arcs in contact *i*.

When deriving expression (21), the following formula is obtained:

$$da_i = \frac{s_i \sin \alpha_2 \cos(\pi - \alpha_{2i} - \delta)}{\sin^2(\pi - \alpha_{2i} - \delta)} d\delta = \frac{a_i}{\tan(\pi - \alpha_{2i} - \delta)} d\delta$$

That is:

$$-\frac{1}{a_i}\frac{da_i}{d\delta} = \frac{1}{\tan(\alpha_{2i} + \delta)}$$

Taking Eq. (16) into account:

$$\kappa_i = \alpha_{2i} + \delta \tag{22}$$

As a result, the geometric interpretation of the average contact angle κ_i is represented in Fig. 6a. This is the angle that is formed by the intersection of the representation plane, the failure plane and the roughness face at the farthest point from the contact.

5.2. Surface roughness geometry by circumference arcs

In this case, the problem is also present in plane deformation, and as in the prior geometry, the plane perpendicular to the joint plane, which contains the direction of the shear force, is represented (Fig. 6b). Angle α_i corresponds to the tangent plane in contact i to create an ideal and symmetrical surface roughness geometry with regard to the mid-plane. With a unit of longitude perpendicular to the plane represented, the following equation is obtained under simple geometric considerations:

$$a_i = s_i \frac{\sin(\alpha_i - \delta)}{\sin \alpha_i} \tag{23}$$

To obtain the value of κ_i, the expression (23) is distinguished and the following is obtained:

$$da_i = \frac{-s_i \cos(\alpha_i - \delta)}{\sin \alpha_i} d\delta = \frac{-a_i}{\tan(\alpha_i - \delta)} d\delta$$

along with:

$$-\frac{1}{a_i}\frac{da_i}{d\delta} = \frac{1}{\tan(\alpha_i - \delta)}$$

Accounting for Eq. (12):

$$\kappa_i = \alpha_i - \delta \tag{24}$$

As in the previous case, the geometric interpretation obtained for the angle κ_i is represented in Fig. 6b. This angle is formed by the representation plane, the failure plane and the roughness tangent at the intersection of both planes and at the farthest point from the contact.

The relationship between the angle in the contact and the average irregularity angle is direct and is shown by $\alpha_i = 2\theta_i$.

5.3. Surface roughness geometry for spherical caps

For a better approach to the study of real joints, it is helpful to consider that surface roughness has a three-dimensional nature; the area of contact between the joint faces is lower than in the case of plane deformation models.

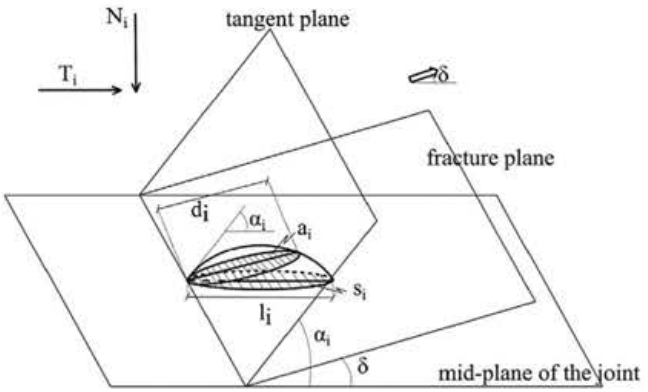

Fig. 7. Three-dimensional surface roughness according to spherical caps in contact *i*.

A failure plane, which defines geometric dilatancy, is assumed to have a maximum slope line in the perpendicular plane to the plane of the joint and to contain the direction of the tangential load to which the discontinuity is subjected.

Fig. 7 represents the evaluated geometry for irregularities. As shown throughout the text, angle α_i serves as the roughness parameter and forms the tangent to the contact in the mid-plane of the joint.

In this case, intersections are circular, and it is necessary to perform the analysis for this particular intersection surface. The diameter of the intersecting circle of the failure plane with the roughness is d_i, and the diameter of the intersecting circle with the roughness in the mid-plane is l_i. This results in:

$$d_i = l_i \frac{\sin(\alpha_i - \delta)}{\sin \alpha_i}$$

And because $a_i = (\pi/4) d_i^2$ and $s_i = (\pi/4) l_i^2$, then:

$$a_i = s_i \frac{\sin^2(\alpha_i - \delta)}{\sin^2 \alpha_i}$$

Taking the derivative of the last equation to obtain the value of κ_i, is follows:

$$da_i = \frac{-2 s_i \sin(\alpha_i - \delta)\cos(\alpha_i - \delta)}{\sin^2 \alpha_i} d\delta = \frac{-2 a_i}{\tan(\alpha_i - \delta)} d\delta$$

and thus:

$$\tan \kappa_i = \frac{\tan(\alpha_i - \delta)}{2} \tag{25}$$

As with the prior case, using the average roughness angle $\theta_i = \alpha_i/2$ can be more practical.

6. Relationship between the *JRC* and the angle of the roughness

The relationship between the theoretical propositions developed herein and the *JRC* used in Barton's formula will be shown.

The geometric variable α_i (or θ_i) will be used to define roughness. To address this question, it will be assumed that the joint profile has more roughness levels and can be treated as a natural fractal. From a physical perspective, a joint experiences fracturing processes that affect the rock at both microscopic and macroscopic levels. The result is a behaviour that follows a fractal structure. The surface roughness of the joint at the microscopic level is caused by intergranular fractures of rock with a roughness scale at the granular level. The macroscopic roughness scale for the joint might be in meters or kilometres.

Mandelbrot [37] suggested measuring the fractal dimension of a particular profile according to the dividing method. The relationship between the total number of divisions N and the dividing longitude r for a particular profile can be expressed as

$$N = Ar^{-D}$$

in which D is the fractal dimension and A is a constant.

Xie and Pariseau [38] considered a joint profile that was statistically similar to the triadic Koch curve (see Fig. 8a), and thus, the generator of the figure was considered with an angle $\theta \in (0,\ 45^{\circ})$. For this model, the fractal dimension D_a was given as

$$D_a = \frac{\ln 2}{\ln(2\ \cos(\theta/2))} \tag{26}$$

To define the fractal dimension, the angle θ can be obtained from a set of m discrete measures in the joint such that:

$$\tan\ \theta = \frac{1}{m}\sum_1^m \frac{2h_i}{b_i} \tag{27}$$

in which h_i and b_i, as defined earlier, are the height and length of each joint roughness, respectively. It is important to note the necessity of considering first-order irregularities in joint strength determinations, as they allow to account for these calculations in the importance of profiles that actually influence the scale of the problem under evaluation (Fig. 8b). The scope of the mathematical formulation presented considers not only the evaluation of the slopes of real roughness of the considered problem, but of the height and length of each joint roughness of laboratory samples. Therefore, the possibility to scale the results of laboratory samples to joints of different sizes, it is not the subject of this investigation.

If the number of roughnesses is elevated and a particular statistical distribution for angle α_i is used (or analogously, angle θ_i):

$$\alpha = \int_{\alpha_0}^{\alpha_f} \alpha_i f(\alpha_i) d\alpha_i$$

Based on the empirical statistical relationship given by Tse and Cruden [39], it is possible to obtain a correlation between *JRC* and the fractal dimension of the established model. The Tse and Cruden function for quantifying joint surface roughness is defined as

$$Z_2 = \frac{1}{\Delta X}\sqrt{\frac{\sum_1^{M-1}(Y_{i+1}-Y_i)^2}{M-1}}$$

such that

$$JRC = 32.20 + 32.47 \log\ Z_2 \tag{28}$$

in which ΔX is the measurement interval in abscissas for the profile in question and $(M-1)$ is the number of intervals into which the profile is divided, such that the extremes of each interval i allow for the definition of measurement points at heights Y_i and Y_{i+1}.

For six established cases with varied heights and longitudes, Xie and Pariseau [38] obtained the following empirical equation in which the Koch triad was defined:

$$JRC = 85.2671(D_a - 1)^{0.5679} \tag{29}$$

These authors obtained good results for estimating *JRC* with this correlation by selecting higher order values of roughness to limit the values of measurable angles in the Barton profiles.

Eq. (29) implies a consideration of the fractal dimension as a measure of joint surface roughness such that the higher the value D_a, the higher the value of *JRC* becomes. For saw-tooth roughness profiles, using the triadic Koch curve appears to be adequate, such that the correlation of Eq. (29) allows to obtain the *JRC* ratio from the angle measured on the basis of the height and length of the roughnesses; thus, *JRC* remains related to the geometric pattern that defines roughness.

To characterise the geometry of irregularities with softened profiles, consequently, is proposed a characterisation of the fractal dimension of the joints with a circumference arc generator that is dependent on the already-defined average contact angle θ with regard to the mid-plane (Fig. 9a), according to a surface roughness geometry formed by circumference arcs. For this model, the following fractal dimension is obtained:

$$D_b = \frac{\ln 3}{\ln(2+(\sin\ 2\theta/2\theta))} \tag{30}$$

This equation is obtained from Fig. 9a, where the overall number of divisions is $N=3$ and the dividing longitude is $r = L_0/L_1 = 2+(\sin 2\theta)/2\theta$.

Analogous to the work performed with the triadic Koch curve fractal, the correlation between the *JRC* and the fractal dimension of the established model can be obtained with the statistical empirical ratio used by Tse and Cruden [39]. A type of joint similar

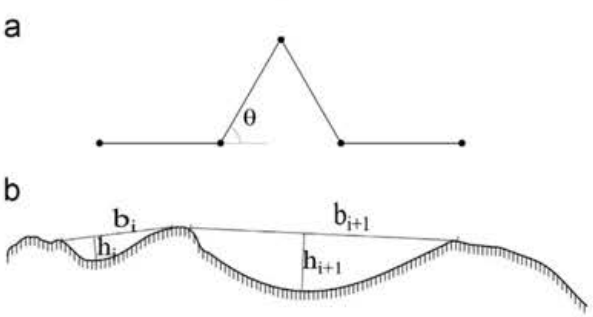

Fig. 8. (a) Xie and Pariseau [38] fractal model; (b) Data needed to determine surface roughness.

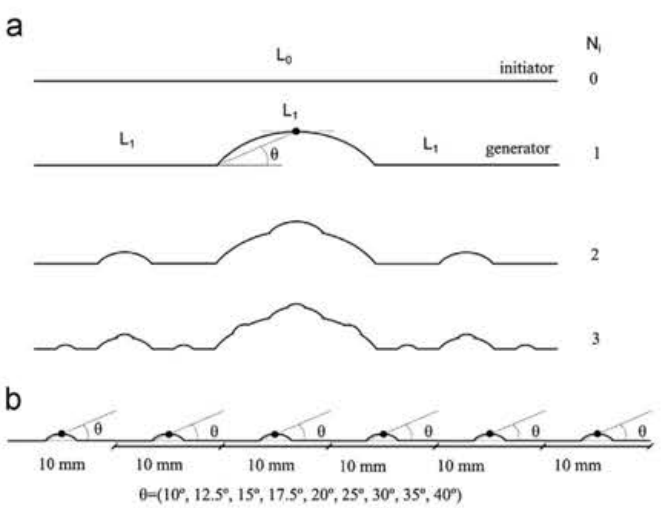

Fig. 9. (a) Fractal generation in circumference arc; (b) Joint model with the circumference arc generator.

Table 1
JRC values corresponding to the average contact angle with roughness according to the type joint model with the circumference arc generator.

Average angle θ	*JRC* Eq. (28)	D_b Eq. (30)
10°	1.68	1.00618
12.5°	4.93	1.00968
15°	7.71	1.01397
17.5°	10.17	1.01907
20°	11.95	1.02499
25°	15.40	1.03934
30°	18.35	1.05716
35°	21.65	1.07862
40°	24.82	1.10389

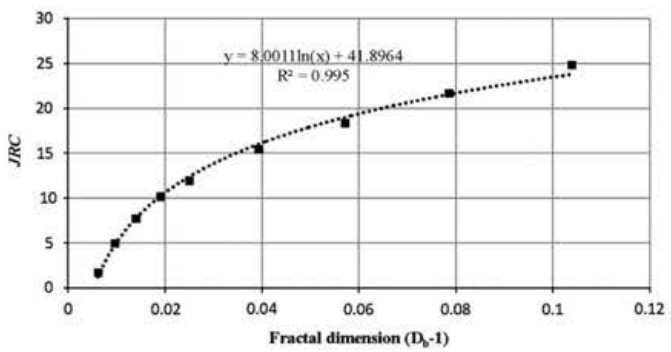

Fig. 10. *JRC* correlation with the fractal dimension of the type joint model with the circumference arc generator.

to that indicated in Fig. 9b can be established in which the angle θ is varied between 10° and 40°. The *JRC* values calculated with Eq. (28) are listed in Table 1, which also includes the results for the fractal dimension obtained with Eq. (30) for the nine established joint profiles.

A regression curve showing the fractal dimension and the obtained *JRC* value is shown in Fig. 10 and has correlation coefficients greater than 0.99. The empirical relationship between the *JRC* value and the fractal dimension for the fractal model defined by Fig. 9a can be expressed using the equation:

$$JRC = 8.0011 \ln(D_b - 1) + 41.8964 \tag{31}$$

It must be remarked that in his semi-empirical law for calculating shear strength, Barton used linear joint profiles to model the three-dimensional effects of joints. In other words, the law not only admits the existence of statistical autosimilarities in any direction but also that the mechanical behaviour of the three-dimensional joint is calculated according to linear surface roughness profiles. In this sense and for the effects of correlations of *JRC* with the geometric parameter that characterises surface roughness, a fractal model for circular arcs has also been developed.

As shown above, Barton's ratio produces elevated joint friction angles when acts very low normal stress values (σ_n). In these cases, the peak friction angle should be limited to the value obtained by Eq. (19). This restriction is identified by mobilising the first failure mechanism, which corresponds to the normal stress below a certain critical value and, according to the theoretical model developed here, satisfies Eq. (4). It is possible to use an equation that connects *JRC* to the fractal dimension by Eqs. (29) and (31) and thus compare the shear strength values obtained for this theoretical model to the value of the peak angle in the semi-empirical formula (20).

Table 2 shows the results that were generated for different average angles over the entire joint that could be estimated as a constant value given by Eq. (27). A basic friction angle of 25° was assumed for the calculations in this table. Values of τ/σ_n that are close to those obtained from Barton's equation were obtained when the value of JRC_a from Eq. (29) and the value of JRC_b from Eq. (31) are used.

Table 2
Estimation of the first failure mechanism according to fractal models and the semi-empirical Barton equation.

Average angle Eq. (27)	D_a Eq. (26)	D_b Eq. (30)	JRC_a Eq. (29)	JRC_b Eq. (31)	$\frac{\tau}{\sigma_n}$ Eq. (4)	$\frac{\tau}{\sigma_n}$ Eq. (20) with JRC_a	$\frac{\tau}{\sigma_n}$ Eq. (20) with JRC_b
10°	1.00553	1.00618	4.46	1.68	0.700	0.639	0.528
20°	1.02259	1.02499	9.91	11.95	1.000	0.896	1.011
30°	1.09859	1.10389	22.88	24.82	2.145	2.041	2.378
40°	1.09859	1.10389	22.88	24.82	2.145	2.041	2.378

7. Influence of intrinsic resistance law of the rock on the contacts

The second shear stress mechanism is associated with the failure of roughness, and thus, it is necessary to incorporate an intrinsic strength criterion with which to model this failure. In some cases, it is possible to study and accept Coulomb's failure criterion. For example, Patton [2] used this criterion to analyse artificially created joints with saw-tooth shapes in gypsiferous material. However, in studies of rocks, it is necessary to use nonlinear failure criteria that allows to consider the influences of confining pressures on shear resistance. Among the existing studies reported in the literature, the most extensive is that developed by Hoek and Brown [40]. The use of this analysis criterion provides a basis for comparison with the semi-empirical Barton model. It is possible to lay a theoretical basis for the determination of the shear strength of discontinuities, and thus, the theoretical formula developed herein includes all of the factors that appear in the experimental equation.

Due to its simplicity, is studied the application of a Coulomb type failure criterion, as well as a Hoek and Brown criterion. An associated flow law is considered in both cases.

7.1. Coulomb's failure criterion for surface roughness

Because Coulomb's law, which includes intrinsic shear strength patterns c and φ, is met in the failure plane, it should also be met by each roughness:

$$\tau_{ri} = c + \sigma_{ri} \tan \varphi \tag{32}$$

Accounting for the expressions that relate the forces on the global axes and those of the failure plane, the following is satisfied:

$$N_i = a_i(\sigma_{ri} \cos \delta - \tau_{ri} \sin \delta)$$

$$T_i = a_i(\sigma_{ri} \sin \delta + \tau_{ri} \cos \delta)$$

If Eq. (15) is deduced for the second mechanism and if the associated flow of the material is assumed, the following ratio is verified for the failure plane for each contact i:

$$\frac{\tau_{ri}}{\sigma_{ri}} = \tan(\varphi + \kappa_i) \tag{33}$$

Substituting Eq. (33) into Eq. (32) for Coulomb failure type, the following is obtained:

$$\sigma_{ri} = c \cos \varphi \frac{\cos(\varphi + \kappa_i)}{\sin \kappa_i}$$

7.2. Application for saw-tooth geometry with symmetrical teeth

For the specific case of saw-tooth geometry in which the teeth are symmetrical, then $\alpha_{1i} = \alpha_{2i} = \alpha_i$, and Eqs. (21) and (22) can be used as follows:

$$\sigma_{ni} = c\ \cos\ \varphi \frac{\sin\ \alpha_i}{\sin^2(\alpha_i + \delta)}\ \cos(\varphi + \alpha_i + 2\delta) \tag{34}$$

$$\tau_i = c\ \cos\ \varphi \frac{\sin\ \alpha_i}{\sin^2(\alpha_i + \delta)}\ \sin(\varphi + \alpha_i + 2\delta)$$

In the stress plane, the intrinsic equations for δ parameters represent a parabola with a focus in the origin and an inclined axis $\varphi - \alpha_i$.

From Eq. (34), it is possible calculate the dilatancy needed to produce the second mechanism for a known normal stress. For the particular case of null dilatancy, the following stress value is obtained:

$$\sigma_{ni}^{\text{crit}} = c\ \cos\ \varphi \frac{\cos(\varphi + \alpha_i)}{\sin\ \alpha_i}$$

For normal stress values above the critical value $\sigma_{ni}{}^{\text{crit}}$, the second mechanism demands a negative dilatancy, which is physically impossible. Thus, the failure is produced with a shear stress that corresponds to a null dilatancy, according to Coulomb's failure criterion, or $\tau_i = \sigma_{ni}\ \tan\ \varphi + c$. For normal stresses below the critical value, the first mechanism gives a lower shear strength than the second, such that $\tau_i = \sigma_{ni}\ \tan(\varphi + \alpha_i)$.

Only one valid point remains in the parabola that arises from the second mechanism, which corresponds to the critical stress in a situation of null dilatancy. The obtained strength law is a bilinear factor (Fig. 11a) identical to that proposed by Patton [2].

7.3. Application for saw-tooth geometry with asymmetrical teeth

If the angle of the contact tooth face is greater than that of the other face ($\alpha_1 > \alpha_2$), then the first mechanism is more resistant than when the teeth are symmetrical at angles α_2. In this case, there is a parabolic section between the two linear laws that corresponds to the second mechanism, where the dilatancy is greater than zero; this represents a modification of Patton's criterion in the central segment. This case is represented in Fig. 11b. In the case of $\alpha_1 < \alpha_2$, the law is again bilinear, as the first strengthening mechanism is flatter than in the symmetrical case of angles α_2, and there is no valid value for the parabola with positive dilatancy (Fig. 11c).

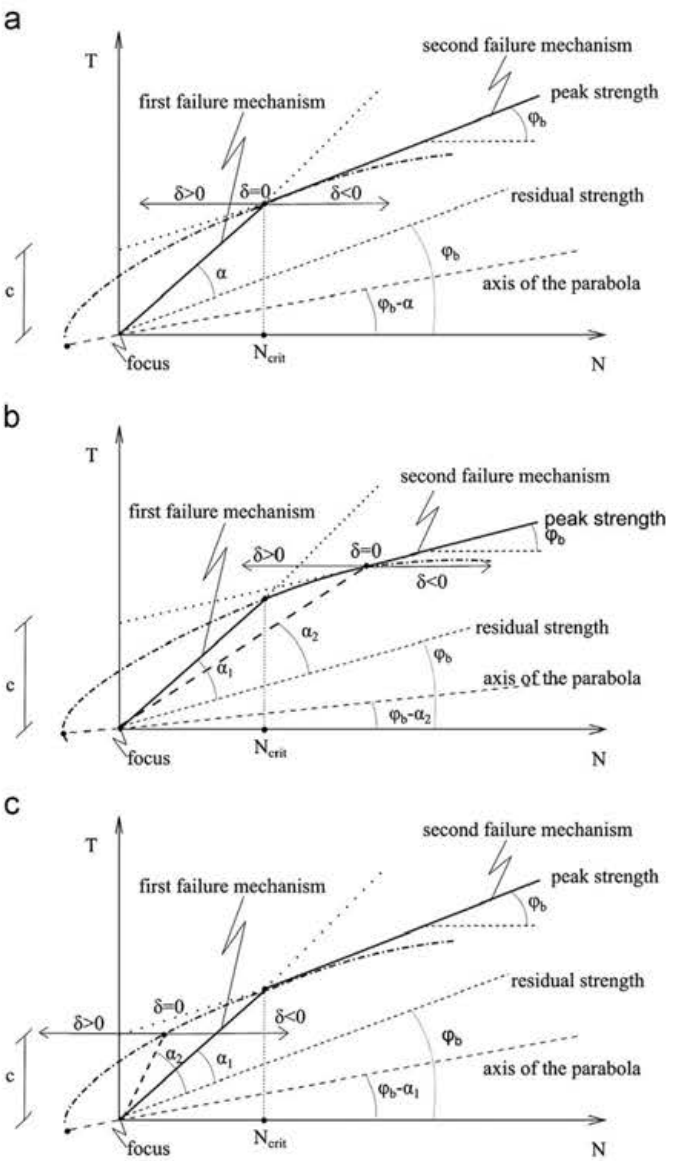

Fig. 11. (a) Strength law for a saw-tooth joint with symmetrical angles and Coulomb's failure criterion; (b) Shear strength behaviour of a saw-tooth joint with angles $\alpha_1 > \alpha_2$ and Coulomb's failure criterion; (c) Shear strength behaviour of a saw-tooth joint with angles $\alpha_1 < \alpha_2$ and Coulomb's failure criterion.

7.4. Hoek and Brown failure criterion for surface roughness

The Hoek and Brown failure criterion [40] with associated flow can be expressed in a parametric form with the angle of instantaneous friction angle as the variable [41], according to equations:

$$\tau_{ri}^* = \frac{\tau_{ri}}{\beta} = \frac{1 - \sin\ \rho}{\tan\ \rho} \tag{35}$$

$$\sigma_{0ri}^* = \frac{\sigma_{ri}}{\beta} + \zeta = \frac{(1 - \sin\ \rho)^2}{2\sin^2\rho}(1 + 2\ \sin\ \rho) \tag{36}$$

in which $\beta = m(\sigma_c/8)$, $\zeta = (8s/m^2)$, and m, s are the Hoek and Brown parameters and σ_c is the uniaxial compressive strength of the rock matrix. The stresses τ_{ri}^* and σ_{0ri}^* are obtained from a dimensionalising and normalising, respectively, the stresses in the failure plane.

The stresses, expressed by Eqs. (35) and (36), are applied to the failure plane if the associated flow law is assumed. However, it is interesting to know these stresses on the mid-plane of the joint; using a Mohr circle, can be obtained the stresses σ_{ni} and τ_i on the desired axes, passing from point R (stresses in the failure plane) to F (stresses in the mid-plane) as indicated in Fig. 12. Therefore:

$$\sigma_{ni} = \sigma_{ri} + \frac{\tau_{ri}}{\cos\ \rho}[\ \sin\ \rho - \ \sin(\rho - 2\delta)]$$

$$\tau_i = \frac{\tau_{ri}}{\cos\ \rho}\ \cos(\rho - 2\delta)$$

By substituting the value of stress in the failure plane of a contact indicated in Eqs. (35) and (36), the following equations are obtained:

$$\sigma_{0ni}^* = \frac{\sigma_{ni}}{\beta} + \zeta = \frac{1}{2\tan^2\rho} - \frac{1 - \sin\ \rho}{\sin\ \rho}\ \sin(\rho - 2\delta) \tag{37}$$

$$\tau_i^* = \frac{\tau_i}{\beta} = \frac{1 - \sin\ \rho}{\sin\ \rho}\ \cos(\rho - 2\delta) \tag{38}$$

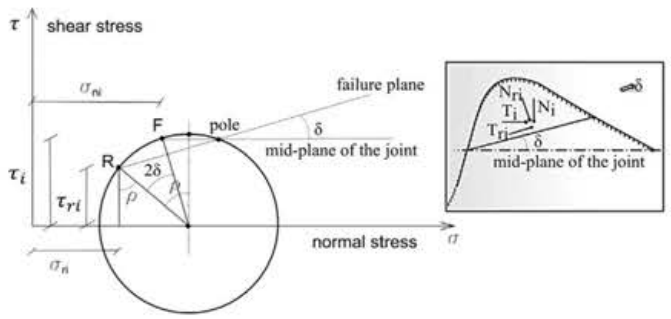

Fig. 12. Obtaining normal stress on the mid-plane of the joint from stress on the failure plane.

Observing the theoretical relationship (15) and the semi-empirical Barton equation, it is interesting to solve for the dilatancy value δ to directly compare both equations. Based on Eq. (37), it is found:

$$\delta = \frac{1}{2}\left[\rho - \operatorname{asin}\left[\frac{\sin\rho}{\sin\rho - 1}\left(\sigma^*_{0ni} - \frac{1}{2\tan^2\rho}\right)\right]\right] \tag{39}$$

Using the Lambe variables $p=(\sigma_1+\sigma_3)/2$ and $q=(\sigma_1-\sigma_3)/2$ and adopting the aforementioned criterion of Serrano and Olalla [41] have shown that:

$$q^* = \frac{q}{\beta} = \frac{1-\sin\rho}{\sin\rho} \tag{40}$$

$$p^*_0 = \frac{p}{\beta} + \zeta = \frac{1}{2\tan^2\rho} \tag{41}$$

By applying (40) and (41) to Eq. (39), it can be obtained:

$$\delta = \frac{1}{2}\left[\rho - \operatorname{asin}\left[\frac{p^*_0 - \sigma^*_{0ni}}{q^*}\right]\right] = \frac{1}{2}\left[\rho - \operatorname{asin}\left[\frac{p-\sigma_{ni}}{q}\right]\right] = \frac{1}{2}[\rho - \operatorname{asin}\eta]$$

with $\eta = (p-\sigma_{ni})/q$.

Consequently, applying the Hoek and Brown failure criterion with associated flow, the strength governing law of the second mechanism is given by Eq. (15) with a dilatancy angle δ to solve the equation:

$$\sin(\rho - 2\delta) = \eta \tag{42}$$

As expected, for a null dilatancy value ($\delta=0$), Eq. (37) shows the failure behaviour exactly as predicted by the Hoek and Brown criterion.

Using the Hoek and Brown failure criterion, the value of the instantaneous friction angle depends on the level of stress such that as the normal load value increases, a smaller angle value is achieved. Based on previous equations, the second mechanism implies a particular representation of the in-plane stresses $\tau-\sigma$ that depends on the Hoek and Brown parameters. When applied to the study of joints, the consideration of these parameters should account for different factors that are difficult to quantify in practice with the criteria normally used for mass rock. In cases of joints, alteration can be incorporated if the assigned value of the basic angle φ_b (or residual φ_r) is used to measure those factors. Thus, it is would consider, as predicted by the Barton formula, that the value of the peak friction angle that defines joint shear strength is reduced to the value of the basic angle if the normal stress is equal to the uniaxial compressive strength of the joint wall.

Equalising the value of the basic friction angle with that predicted by the second failure mechanism for a normal stress on the joint, σ_n equal to σ_c, and demonstrating that the dilatancy angle is positive, it is possible obtain the value of the parameter m according to the Hoek and Brown criterion from the following equation:

$$\varphi_b = (\rho + \kappa_m + \delta)_{\sigma_n = \sigma_c} \tag{43}$$

In the case of null dilatancy, failure at that stress value would be directly indicated by the Hoek and Brown criterion, and it would be possible obtain the value of the parameter m that would permit obtaining a tangential stress equal to $\sigma_c \tan\varphi_b$.

Taking into account Eq. (38), the expression of Lambe's parameter q from Eq. (40) and the obtained ratio (42), it is possible construct an equation that represents the strength law of the joint for the second failure mechanism:

$$\frac{\tau}{\sigma_n} = \frac{q}{\sigma_n}\sqrt{1-\eta^2} \tag{44}$$

It is necessary to employ the Hoek and Brown criterion parameters when using this expression. Eq. (44) demonstrates that the law of joint strength, expressed as a function of the relationship between the stresses acting on the joint walls, depends on the normal stress that acts on the joint, the instantaneous friction angle and on the Hoek and Brown criterion parameters. As shown above and according to Eq. (43), these parameters depend on surface roughness characteristics and the state of joint alteration. This dependence presents a clear analogy to the dependence terms in the Barton semi-empirical formula.

The dependence of the instantaneous friction angle with the normal stress can be easily expressed based on Eqs. (37) and (38), as well as Eq. (15). For the entire joint, the following is obtained:

$$\sigma_n^2(1+\tan^2(\rho+\kappa_m+\delta)) - 2p\sigma_n + p^2 - q^2 = 0 \tag{45}$$

By evaluating the dilatancy angle δ from Eq. (39) applied to the entire joint. Based on the above expressions, it is possible to obtain specific equations for each type of modelled roughness.

8. Practical application: Example

The most realistic case is that of geometrical modelling with spherical caps. From this hypothesis, the equations for shear strength can be obtained. The first mechanism is formulated by the equation:

$$\frac{\tau}{\sigma_n} = \tan(\alpha + \varphi_b) \tag{46}$$

This expression is applied to all roughness geometries for which angle α is evaluated according to (5) and (6) while considering each average contact angle (that is $\alpha_i = \theta_i$).

For the second mechanism, it is important to remember that to approach the study of three-dimensional joints, Eq. (25) must be considered because it defines the reduction angle of the contact. It is necessary to solve the nonlinear equation system that is composed of Eq. (39) (applied to the entire joint), (44) and (45). The value of the reduction angle of the contact for the entire joint can be evaluated as

$$\kappa_m = \operatorname{atan}\left[\frac{s_t}{\sum_1^n (2s_i/(\tan(\alpha_i - \delta)))}\right] \tag{47}$$

Or the expression of Eq. (47) in its integral form if distribution functions are considered.

It is also necessary to evaluate the values for m and s while taking into account the m_0 value corresponding to the intact rock and considering alteration when applying this value to the condition of the joint walls according to Eq. (43). The s value can be obtained as follows:

$$s = \left(\frac{m}{m_0}\right)^{\frac{28}{9}}$$

An application of the Hoek and Brown criterion equations for defining joint strength corresponding to situations in which

solving the second mechanism by equations leads to negative geometric dilatancy angles. Because such angles are not physically possible, such situations require the proposal of null dilatancy and thus a direct application of the failure criterion equations.

There are three zones that contribute to the strengthening behaviour of a joint that is subjected to shear force. The first zone corresponds to the first mechanism, which is produced until Eq. (15) is equal to (46). This situation is produced for an instantaneous friction angle equal to:

$$\rho = \frac{\alpha}{2} + \varphi_b - \delta - \operatorname{atan}\left[\frac{s_t}{\sum_1^n (2s_i/(\tan(\alpha_i - \delta)))}\right] \tag{48}$$

In the second zone, in cases of decreasing dilatancy values, the second mechanism equations govern until the dilatancy reaches zero. This occurs for an instantaneous friction angle such that [41]:

$$2\sin^3\rho - (2\sigma_{0n}^* + 3)\sin^2\rho + 1 = 0 \tag{49}$$

Finally, the third zone is given, from the previous point, by Eqs. (35) and (36).

In Figs. 13–15, the shear strength governing law for some of the values indicated in the theoretical model parameters are analyzed considering equal three-dimensional roughnesses and the Hoek and Brown failure criterion. These representations also show the shear strength governing law that was deduced when the Barton criterion was applied with the *JRC* value, according to (31). These graphs allow the comparison of both models, for different values of m_0 and α, and a residual friction angle value of 30° in all cases.

According to the application of the above-described equations, these figures show the three zones that delimit the shear strength governing law until a value of 20 MPa is achieved for the joint wall uniaxial compressive strength. Low observed values for the angle that defines roughness and for the m_0 parameter imply the appearance of a broad zone for the second failure mechanism, with a null dilatancy zone for high levels of roughness and m_0.

As observed in the depicted graphs, the theoretical model developed herein produces higher values than those obtained with the Barton method. This finding shows that at lower normal stresses, the peak strength angle is higher than that obtained with the Barton's theory. Additionally, the results obtained with higher angles for the roughness demonstrate that low normal stress values greatly affect at the roughness via degradation. It is common to arrive at null dilatancy and be governed by the rock failure criterion for estimations of joint behaviour. At lower roughness angles, the normal load applied to the joint has less initial effect, although its strength would be lower. Thus, in these situations, the nonzero dilatancy zone achieves high values of normal stress and increases the contribution of the second mechanism. As observed, high m_0 values more strongly affect the behaviour of surface roughness and result in a null dilatancy zone for low normal stress values.

A similar study of surface roughness could be performed as suggested geometrically in Section 3. It can be appreciated that linear joints do not optimally represent three-dimensional behaviour, and thus, it is not possible to obtain reasonable values with the Hoek and Brown parameters for determining a roughness failure mechanism. This is mainly because linear joint models, such as the saw-tooth or circumference arcs, imply a greater area of contact between the contact surfaces and overestimate the peak strength above realistic values and above those obtained for three-dimensional geometries. Consequently, null dilatancy situations appear very easily in almost all ranges of parameters assigned to the model, which reduces the study to the first mechanism and

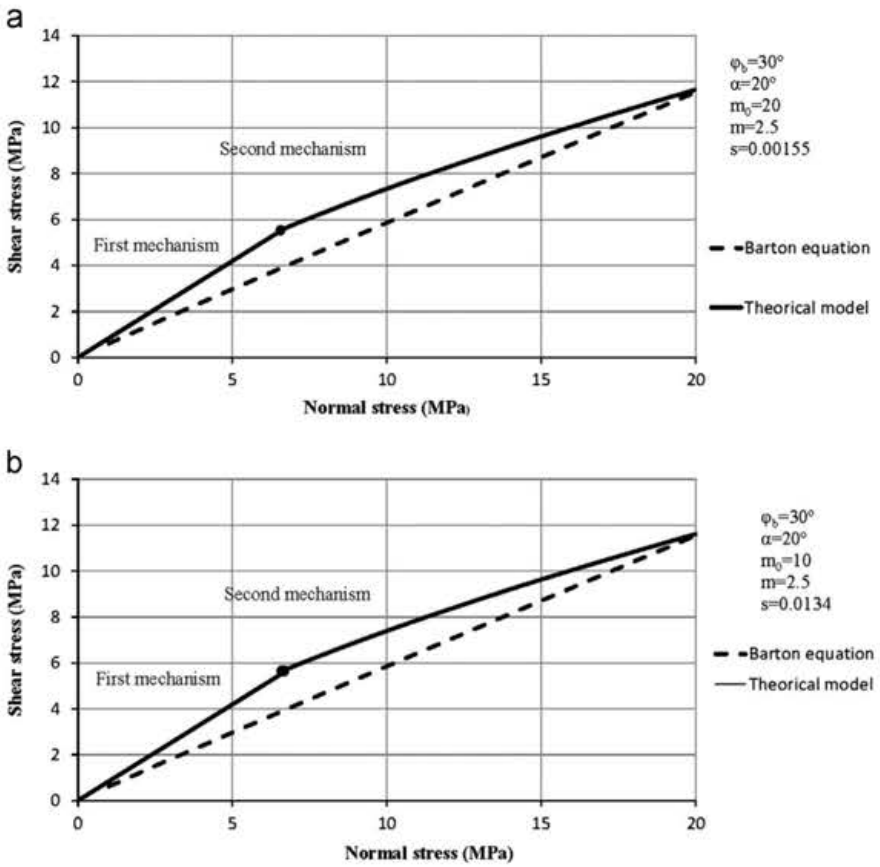

Fig. 13. (a) Shear strength governing law according to the theoretical and experimental Barton model for $\varphi_b = 30°$, $m_0 = 20$ y $\alpha = 20°$; (b) Shear strength governing law according to the theoretical and experimental Barton model for $\varphi_b = 30°$, $m_0 = 10$ y $\alpha = 20°$.

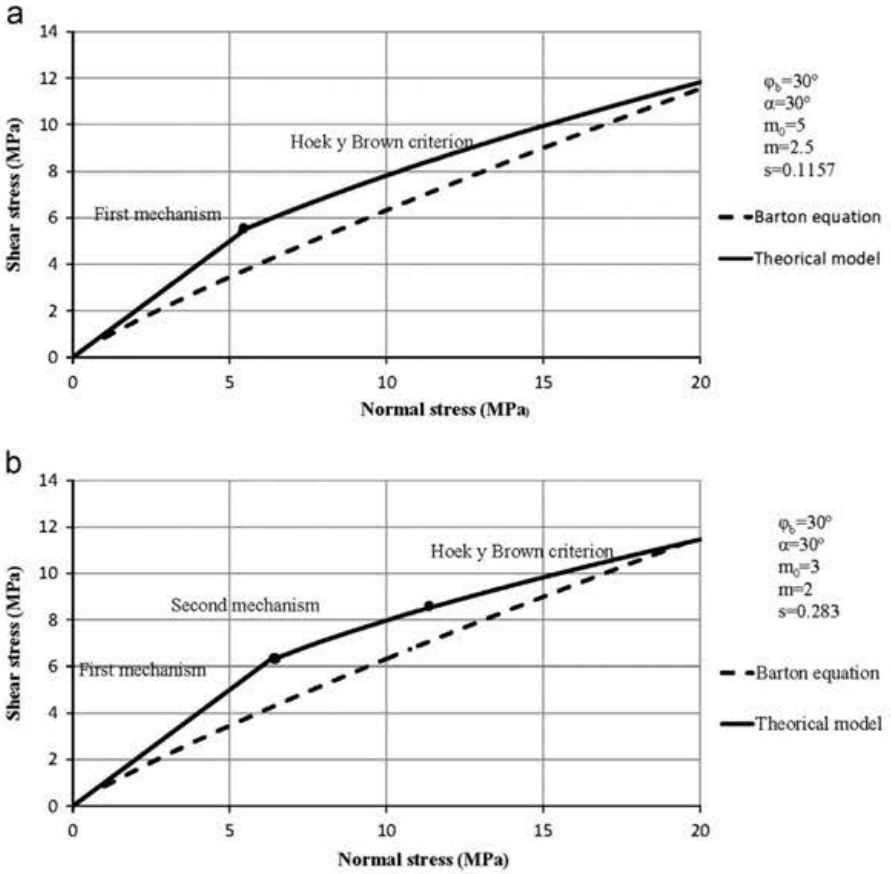

Fig. 14. (a) Shear strength governing law according to the theoretical and experimental Barton model for $\varphi_b=30^\circ$, $m_0=5$ y $\alpha=30^\circ$; (b) Shear strength governing law according to the theoretical and experimental Barton model for $\varphi_b=30^\circ$, $m_0=3$ y $\alpha=30^\circ$.

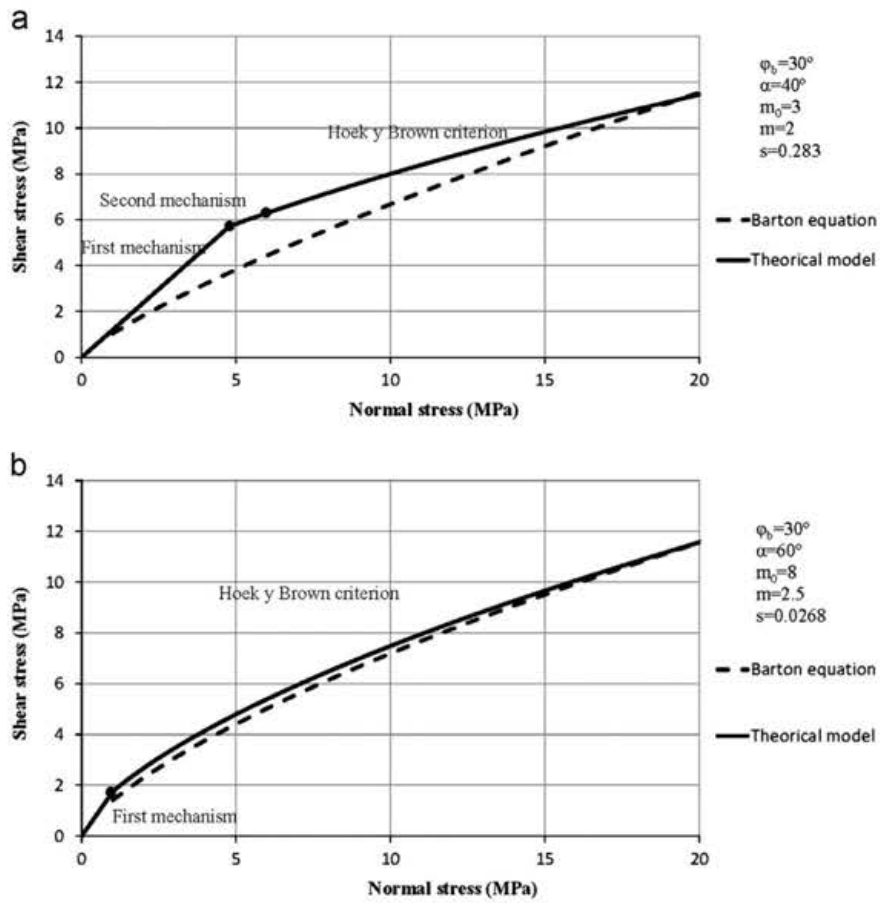

Fig. 15. (a) Shear strength governing law according to the theoretical and experimental Barton model for $\varphi_b=30^\circ$, $m_0=3$ y $\alpha=40^\circ$; (b) Shear strength governing law according to the theoretical and experimental Barton model for $\varphi_b=30^\circ$, $m_0=8$ y $\alpha=60^\circ$.

the failure criterion. As a result, these studies cannot represent situations of dilatancy via asperities failure.

In the particular case of surface roughness geometry according to circumference arcs, it must be noted that Eq. (45) can be expressed as

$$\sigma_n^2(1+\tan^2(\alpha_m+\rho))-2p\sigma_n+p^2-q^2=0 \tag{50}$$

in which is defined the value of angle $\alpha_m=\kappa_m+\delta$, obtaining κ_m from Eqs. (16) (or 17) and (24).

In this case, uniform roughness is assumed for the entire profile with a constant roughness angle α. Thus, Eq. (50) does not depend on the dilatancy angle, and the influence of this angle on the shear strength governing laws is only given by obtaining the Hoek and Brown parameter for equality (43) and by demonstrating that this angle is positive and lower than α, i.e., physically possible.

9. Methodology for estimating the shear strength of a joint

Based on the study described herein, a method of estimating the joint strength according to the theoretical analysis is shown. Initially, first-order surface roughness is geometrically characterised in the joint to be studied by obtaining the relationship between the height and half-length measure on the mid-plane. In other words, previous knowledge of the roughness profile of the joint surface is required. Thus, an expected α value can be obtained from the sample. It is possible also obtain this value more rigorously on the basis of a particular distribution function for average contact angles that represent the characterisation of the roughness values of the studied joint.

Three-dimensional roughness is considered to be the best alternative (option 5.c). Consequently, the expected value for the contact area reduction angle κ_m is obtained for a three-dimensional roughness geometry using formula (16) and (17).

The m_0 parameter from Hoek and Brown must be assigned, as well as the uniaxial compressive strength for the rock. It is also necessary to estimate the value of the basic friction angle for the surface of the joint. The value of m is calculated by applying the Hoek and Brown model such that the peak angle evaluated via the second mechanism equals the basic friction angle of the joint for the point at which the normal stress equals the uniaxial compression strength for the joint wall (Eq. (43)). Because the failure and negative values for dilatancy angles are not physically possible in this situation, a null dilatancy zone and the failure criterion are used.

Eq. (46) is used for the first failure mechanism until the friction angle reaches the value indicated in (48). For values above this angle, Eq. (39) is used for the entire joint, along with (44) and (45). These equations govern joint failure behaviour according to the second mechanism and are used until dilatancy reaches zero (a situation that will occur if the instantaneous friction angle is achieved, according to (49)); the Hoek and Brown failure criterion is used to estimate joint strength with higher normal stresses (Eqs. (35) and (36)).

The obtained theoretical results can be compared with the method developed herein with the semi-empirical Barton's theory. A *JRC* value can be adopted according to the correlation of Eq. (31) with the fractal dimension calculated by Eq. (30) for average contact angles, such that angle $\theta=\alpha$ is used.

10. Conclusions

This study allows the establishment of theoretical basis for the elaboration of the criterion of shear strength for rock discontinuities. Two failure mechanisms are identified in accordance with the normal load level acting at the joint. Both mechanisms have clear physical interpretations and are supported by empirical evidence collected in numerous studies. The first mechanism appears for low normal stresses and corresponds with slippage between the faces of each joint wall. When acting normal stress is high, the second failure mechanism occurs, which corresponds to a failure of contacts due to the plastification of roughness. Both mechanisms are theoretically analysed and their behaviour is according to Eqs. (4) and (15).

The influence of surface roughness has been characterised by defining simple geometric parameters. Particularly, the average contact angle θ for roughness is calculated. It is easily measurable in both field and laboratory. It is defined as the angle for which tangent is the roughness height divided by the half-length at the mid-plane that is covered by the surface roughness.

Using this parameter, different assumed roughness geometries have been characterised. Particularly, for an approach to the three-dimensional study of joints, the use of irregularities such as spherical caps on the joint mid-plane, is recommended. Additionally, saw-tooth surfaces and circumference arcs have been also analysed. For characterisations of surface roughness, a particular fractal dimension has been defined to indicate self-similarity at different roughness levels. First-order roughness should be considered when determining the effects on joint strength according to the length of the joint. Using the Hoek and Brown failure criterion [40] to characterise failure via the contact of irregularities according to the second mechanism, it is possible to calculate joint strength depending on the relationship between the actions of normal stress and uniaxial compressive strength.

In the case of this second mechanism, the obtained theoretical formula has the same structure as the relationship reported by Barton (18). The theory presented herein indicates that the geometric dilatancy, the surface roughness geometry and the instantaneous friction angle are the factors governing the behaviour at failure. They have a direct relationship to φ_b, *JRC* and *JCS* parameters of Barton's formula.

The fractal characterisation of surface roughness has revealed a relationship between this roughness state and the *JRC* defined in the Barton empirical formula (Eq. (31)). The theoretical formula described depends on dilatancy, the instantaneous friction angle, the relationship between normal stress and uniaxial compressive stress and the roughness, as defined in the above-mentioned theoretical case based on the angle θ.

A theoretical model for both formulated mechanisms has been applied to Coulomb's failure criterion, as defined for saw-tooth geometry. The result for symmetrical teeth was the bilinear curve obtained by Patton in 1966 [2]. However, it must be noted that the asymmetry of the serrated edges (saw-tooth) could lead to an agreement of both mechanisms through second-order parabolas.

The described theoretical formula was applied to the Hoek and Brown failure criterion for three-dimensional roughness geometries and resulted in more realistic strength values than those obtained for the case of linear surface roughness. In this ultimate case, values are much higher than those deduced from Barton [1] due to a greater area of contact between surfaces of broken roughness. The theoretical formula presented herein could be used to study the shear strength of rock joints based in non-empirical assumptions by a relatively simple and practical analysis process.

References

Barton N. Review of a new shear strength criterion for rock joints. Eng Geol 1973;7:287–332.
Patton FD. Multiple modes of shear failure in rock. In: Proceedings of the first congress of international society of rock mechanics, Lisbon; 1966. p. 509-513.

Newland PL, Alley BH. Volume changes in drained triaxial tests on granular materials. Geotechnique 1957;7:17–34.
Ladanyi B, Archambault G. Simulations of the shear behavior of a jointed rock mass. In: Proceedings 11th US symposium on rock mechanics, Berkeley; 1970. pp. 105–125.
Jaeger JC. Friction of rocks and stability of rock slopes. Geothecnique 1971;21 (2):97 (–34).
Schneider HJ. The friction and deformation behavior of rock joints. Rock Mech Rock Eng 1976;8:169–84.
Heuze FE, Barbour TG. New models for rock joints and interfaces. ASCE J Geotech Eng Div 1982;108(5):757–76.
Leichnitz W. Mechanical properties of rock joints. Int J Rock Mech Min Sci 1985;22(5):313–21.
Plesha ME. Constitutive models for rock discontinuities with dilatancy and surface degradation. Int J Numer Anal Methods Geomech 1987;11:345–62.
Zubelewicz A, O'Connor K, Dowding CH, Belytschko T, Plesha ME. A constitutive model for cyclic behavior of dilatant rock joints. In: Proceedings second international conference on constitutive laws for engineering materials, Arizona; 1987. pp. 1137–1144.
Qiu X, Plesha ME, Huang X, Haimson BC. An investigation of the mechanics of rock joints—Part II: Analytical investigation. Int J Rock Mech Min Sci 1993;30 (3):271–87.
Saeb S, Amadei B. Modeling rock joints under shear and normal loading. Int J Rock Mech Min Sci 1992;29:267–78.
Seidel JP, Haberfield CM. The application of energy principles to the determination of the sliding resistance of rock joints. Rock Mech Rock Eng 1995;28 (4):211–26.
Hutson RW. Preparation of duplicate rock joints and their changing dilatancy under cyclic shear. Evanston: Northwestern University; 1987 (PhD Thesis).
Hutson RW, Dowding CH. Joint asperity degradation during cyclic shear. Int J Rock Mech Min Sci 1990;27(2):109–19.
Huang X, Haimson BC, Plesha ME, Qui X. An investigation of the mechanics of rock joints—Part I. Laboratory investigation. Int J Rock Mech Min Sci 1993;30:257–69.
Lee HS, Park YJ, Cho TF, You KH. Influence of asperity degradation on the mechanical behavior of rough rock joints under cyclic shear loading. Int J Rock Mech Min Sci 2001;38:976–80.
Homand F, Lefevre F, Belem T, Souley M. Rock joints behaviour under cyclic direct shear tests. In: Amadei K, Smealie, Scott, editors. Rock mechanics for industry. Rotterdam: Balkema; 1990. p. 399–406.
Gens A, Carol I, Alonso EE. A constitutive model for rock joints, formulation and numerical implementation. Comput Geotech 1990;9:3–20.
Desai CS, Fishman KL. Plasticity-based constitutive model with associated testing for joints. Int J Rock Mech Min Sci 1991;28(1):15–26.
Grasselli G, Egger P. Constitutive law for the shear strength of rock joints based on three-dimensional surface parameters. Int J Rock Mech Min Sci 2003;40:25–40.
Belem T, Souley M, Homand F. Modelling surface roughness degradation of rock joint wall during monotonic and cyclic shearing. Acta Geotech 2007;2: 227–48.
Samadhiya NK, Viladkar MN, Al-Obaydi MA. Three-dimensional joint/interface element for rough undulating major discontinuities in rock masses. Int J Geomech 2008;8(6):327–35.
Barton N. Rock mechanics review: the shear strength of rock and rock joints. Int J Rock Mech Min Sci 1976;13:255–79.
Barton N, Choubey V. The shear strength of rock joints in theory and practice. Rock Mech Rock Eng 1977;10:1–54.
Lee YH, Carr JR, Barr DJ, Haas CJ. The fractal dimension as a measure of the roughness of rock discontinuity profiles. Int J Rock Mech Min Sci 1990;27:453–64.
Huang SL, Oelfke SM, Speck RC. Applicability of fractal characterization and modelling to rock joint profile. Int J Rock Mech Min Sci 1992;29:89 (–8).
Den Outer A, Kaashoek JF, Hack HRGK. Difficulties with using continuous fractal theory for discontinuity surfaces. Int J Rock Mech Min Sci 1995;32:3–9.
Muralha J. Fractal dimension of joint roughness surfaces. In: Proceedings fractured and jointed rock masses, Rotterdam; 1995. p. 205-12.
Xie H, Wang JA, Kwasniewski MA. Multifractal characterization of rock fracture surfaces. Int J Rock Mech Min Sci 1999;36:19 (–7).
Reeves MJ. Rock surface roughness and frictional strength. Int J Rock Mech Min Sci 1985;22:429–42.
Asadollahi P. Stability analysis of a single three dimensional rock block: effect of dilatancy and high-velocity water jet impact. Austin: University of Texas; 2009 (PhD Thesis).
Terzaghi K. Erdbaumechanik. Leipzig: Franz Deuticke; 1925.
Hertz H. On the contact of rigid elastic solids and on hardness. New York: Macmillan; 1882.
Barton N, Bandis S. Effects of block size on the shear behavior of jointed rock. In: Proceedings of the 23rd US symposium on rock mechanics, Berkeley, California; 1982.
Dickey JW. Frictional characteristis of quartz. Cambridge: MIT; 1966 (PhD Thesis).
Mandelbrot BB. The fractal geometry of nature. New York: Freeman; 1982.
Xie H, Pariseau WG. Fractal estimation of joint roughness coefficients. In: Proceedings of the conference on fractured and jointed rock masses, Lake Tahoe, California; 3–5 June 1992; 1992. p. 125–131.
Tse R, Cruden DM. Estimating joint roughness coefficients. Int J Rock Mech Min Sci 1979;16:303–7.
Hoek E, Brown ET. Empirical strength criterion for rock masses. ASCE J Geotech Eng Div 1980;106(9):1013–35.
Serrano A, Olalla C. Ultimate bearing capacity of rock masses. Int J Rock Mech Min Sci 1994;31(2):93 (–06).